

MASSIVE STAR FORMATION AND SUPERWINDS IN IRAS 19254–7245 (THE “SUPERANTENNAE”)

LUIS COLINA,¹ SEBASTIAN LÍPARI,^{2,3,4} AND F. MACCHETTO⁵
 Space Telescope Science Institute

Received 1991 January 17; accepted 1991 April 5

ABSTRACT

The ultraluminous *IRAS* galaxy IRAS 19254–7245 is investigated by means of aperture spectroscopy and images. It shows the spectral characteristics of a Seyfert 2–type galaxy with the emission lines split into four independent kinematical components separated by a velocity of 1491 km s⁻¹.

A heavy internal obscuration corresponding to $E(B-V) = 1.40$ and a total amount of ionized gas equal to $M_g = 1.1 \times 10^8 M_\odot$ have been measured in the circumnuclear emission-line regions. The upper limit to the total dust mass is $M_d = 1.5 \times 10^7 M_\odot$ and the corresponding cold gas mass is $M_{\text{cg}} = 3.0 \times 10^9 M_\odot$, while the total amount of molecular gas detected in the whole system is $M_{\text{H}_2} = 3.0 \times 10^{10} M_\odot$.

The optical morphology shows a distorted main body composed of two differentiated nuclei separated by about 10 kpc while two long tails extending over a total size of 305 kpc in projection are also detected. The measured amounts of cold gas and dust together with the extraordinarily large size of the tails indicate that IRAS 19254–7245 is the merger of two almost equally massive gas-rich spiral galaxies and that the merging process did start 10⁹ yr ago.

The line splitting is interpreted as produced in a biconical outflow characterized by an opening angle of around 80°, an inclination of the symmetry axis with respect to our line-of-sight of 73°, and flow velocity of 800 km s⁻¹. The total kinetic energy of this outflow amounts to $E_k = 0.5 M_g V_{\text{flow}} = 1.4 \times 10^{57}$ ergs and is explained as produced by supernova explosions and stellar mass loss winds generated during a process of steady star formation with $\text{SFR} = 150 M_\odot \text{ yr}^{-1}$ over a time scale of $t_{\text{SFR}} = 2 \times 10^7$ yr.

The amount and energy distribution of the ionizing photons generated in the star formation process are sufficient to account for the large infrared and H α luminosities, while the shape of the spectrum is not hard enough to explain the Seyfert 2–type excitation conditions. These properties are interpreted under the scenario of a quasar-type central nucleus obscured by a huge amount of gas/dust clouds where the massive star formation is taking place.

Subject headings: galaxies: individual (IRAS 19254–7245) — galaxies: interactions — galaxies: internal motions — galaxies: Seyfert — infrared: sources — stars: formation — quasars

1. INTRODUCTION

High-luminosity infrared galaxies ($L_{\text{IR}} \geq 10^{11} L_\odot$) have been the subject of numerous investigations over the past few years since their discovery by the *IRAS* satellite. The main reason is that they are the best targets to study the relationship between galaxy interactions, enhanced circumnuclear star formation (see Heckman 1990 for a review), and possibly to investigate the creation of a massive black hole in the nucleus of these galaxies.

Recent imaging surveys show that about 46% \pm 12% of the high-luminosity *IRAS* galaxies are in interacting systems (Lawrence et al. 1989), while for the subsample of ultraluminous *IRAS* galaxies ($L_{\text{IR}} \geq 10^{12} L_\odot$) this number increases up to 100% (Sanders et al. 1988; Melnick & Mirabel 1990).

Spectroscopic surveys (Armus, Heckman, & Miley 1989; Leech et al. 1989; Sanders et al. 1988) show that the excitation mechanisms present in these galaxies change as the infrared luminosity increases. While 90% of the moderate-luminosity

($10^{10} \leq L_{\text{IR}} \leq 10^{11} L_\odot$) and 70% of the high-luminosity ($10^{11} \leq L_{\text{IR}} \leq 10^{12} L_\odot$) *IRAS* galaxies have an H II region–like emission-line spectrum (Leech et al. 1989), 90% of the ultraluminous galaxies ($L_{\text{IR}} \geq 10^{12} L_\odot$) show a Seyfert2/LINER emission-line spectra (Sanders et al. 1988).

Extraordinarily large star formation rates amounting up to a few hundred solar masses per year and superwinds with velocities of the order of 500 km s⁻¹, originating in supernova explosions and mass-loss winds in massive stars, have recently been invoked to explain the double-peaked line profiles, the emission-line ratios, and the energy budget in high-luminous *IRAS* galaxies (Heckman, Armus, & Miley 1990).

IRAS 19254–7245 is an ultraluminous infrared galaxy ($L_{\text{IR}} = 1.1 \times 10^{12} L_\odot$; Melnick & Mirabel 1990) located at a redshift of $z = 0.0616$ and detected in the survey of southern warm *IRAS* AGN candidates (Lipari, Bonatto, & Pastoriza 1989, 1990; Lipari, Macchetto, & Golombek 1991). Broad-band NTT images of this galaxy (Melnick & Mirabel 1990) show the presence of two nuclei separated by a projected distance of around 9" and showing evident signs of being in an advanced stage of merger. These authors also reported the presence of a huge amount of molecular gas $M_{\text{CO}} = 3 \times 10^{10} M_\odot$ (10 times larger than the molecular gas content in our Galaxy) that could act as a reservoir for a large star formation rate.

¹ Dpto. de Física Teórica, Univ. Autónoma, Madrid, Spain.

² Córdoba Observatory, Córdoba, Argentina.

³ Visiting Astronomer at CASLEO Observatory.

⁴ Member of the Carrera del Investigador, CONICET, Argentina.

⁵ Affiliated to the Astrophysics Division, ESA-ESTEC, Noordwijk, The Netherlands.

In this paper we present (§ 2) the first aperture spectroscopy around the two optical nuclei of IRAS 19254–7245 together with an image of the 3.75×3.75 region around this galaxy. The results, mainly the amount of dust and ionized gas, the evidence of kinematically independent emission-line components, and the excitation mechanisms are presented in § 3. Interpretation of the results in terms of a merger of two gas-rich galaxies, large star formation rates, presence of superwinds, and obscured nonthermal ionizing source are discussed in § 4. Throughout the paper a Hubble constant of $H_0 = 75 \text{ km s}^{-1} \text{ Mpc}^{-1}$ will be assumed.

2. OBSERVATIONS AND REDUCTIONS

The spectroscopic observations of IRAS 19254–7245 reported in this work were obtained with the “Z-machine” (Tonry & Davis 1979; Latham 1982; da Costa et al. 1984) attached to the Cassegrain spectrograph at the 2.15 m Ritchey-Chrétien telescope of CASLEO, San Juan, Argentina. The data were obtained during four photometric nights in the period 1989 June to 1990 June. A journal of the observations is given in Table 1.

The observations were made using a 600 line mm^{-1} grating, giving a dispersion of 120 \AA mm^{-1} , an effective resolution of 5 \AA , and covering the wavelength range from 4700 to 7200 \AA . The measurements were made through a pair of $3'' \times 6''$ entrance apertures separated by $37''$ on the sky for simultaneous object and sky exposures. The detector employs a dual 936 Reticon system coupled to a high-gain image tube package. A complete object exposure consists of two equal time exposures with the source placed on each of the two channels. In order to obtain a reliable pixel wavelength solution, comparison exposures were made, just before and after the object. Usually, 50–60 He-Ne-Ar and sky lines were used in a seventh-order polynomial fit of the wavelength solution with typical rms residuals of 0.4 \AA . Incandescent lamp exposures were taken at the end of each night to remove the fixed noise pattern arising in the readout electronics (Davis & Latham 1979).

The spectra were flux calibrated with stars from the catalog of southern spectrophotometric standards (Stone & Baldwin 1983). We estimated the galactic reddening as $E(B-V) = 0.13$ by looking for “neighboring” objects in the catalogs of Sandage & Tammann (1981) and de Vaucouleurs, de Vaucouleurs, & Corwin (1976). Each spectrum was separately corrected for Galactic reddening and redshift. In order to increase the signal-to-noise ratio, the corrected spectra were later averaged for the final detailed study. The IRAF package at the STScI was used to measure the spectra. Also, the emission lines

were decomposed using Gaussian profiles by means of a nonlinear least-squares algorithm described in Bevington (1969); the convergence criterium was the minimization of the reduced χ^2 .

3. RESULTS

3.1. Optical Morphology

A digitized image of the optical counterpart of IRAS 19254–7245 and its 3.75×3.75 surroundings ($250 \times 250 \text{ kpc}$ at the IRAS 19254–7245 redshift) is shown in Figure 1 (Plate 1). This image was obtained using the Guide Star Astrometric Package (GASP) at STScI. The main body of the galaxy is formed by two nuclei (more clearly visible in the CCD images of Melnick & Mirabel 1990 and in our own unpublished images) separated in projection by around $9''$ (i.e. 10.5 kpc). Of the two nuclei, the southern one has a Seyfert 2-type spectrum (see Fig. 2a) and agrees in position with the peak of the IRAS source. The northern nucleus also shows $H\alpha$ and $[\text{N II}]$ in emission (see Fig. 2b) but at a much lower level.

The optical galaxy has also two extraordinarily long and thin tails having a total size in projection of the order of 300 kpc (see also the deep CCD image in Melnick & Mirabel 1990). The southern tail is the longer with a size of 178 kpc , while the northern tail has a slightly smaller size of around 127 kpc . Finally, there is evidence for condensations located at different positions all along the tails. These could be associated with regions of star formation (see Fig. 1).

The whole optical morphology of the galaxy IRAS 19254–7245 is similar to that detected in classical archetypes of galaxies in interaction/merging like the “Antennae” (Toomre & Toomre 1972) or Arp 226 (also NGC 7252; Schweizer 1982; Borne & Richstone 1991) but at even larger scale. This morphology, distorted main body with multiple nuclei and long tails, is also characteristic of all ultraluminous galaxies (Sanders et al. 1988; Melnick & Mirabel 1990) and has also been observed in Markarian galaxies with multiple active nucleus (Fricke & Kollatschny 1989).

3.2. Amount and Distribution of Dust

The internal extinction within the emission line regions has been measured using the observed $H\alpha/H\beta$ ratio and comparing this with the theoretically predicted value for recombination case B with an electron temperature $T_e = 1.5 \times 10^4 \text{ K}$ and low electron density. The value obtained in this way $E(B-V) = 1.40$ is similar to the mean value $E(B-V) = 1.53 \pm 0.62$ measured in a sample of nine ultraluminous infrared galaxies (Sanders et al. 1988).

TABLE 1
JOURNAL OF THE OBSERVATIONS OF IRAS 19254–7245

Date	Instrument	Band	Exposure Time (s)	Comments
1989 Jun 29.....	CASLEO 2.15 m	$\lambda\lambda 4700\text{--}7200$	2400	PA 90° : southern nucleus
1989 Aug 31.....	CASLEO 2.15 m	$\lambda\lambda 4700\text{--}7200$	2400	PA 90° : southern nucleus
		$\lambda\lambda 4700\text{--}7200$	2000	PA 90° : northern nucleus
1990 Jun 23.....	CASLEO 2.15 m	$\lambda\lambda 4700\text{--}7200$	4800	PA 90° : southern nucleus
		$\lambda\lambda 4700\text{--}7200$	3000	PA 90° : northern nucleus
1990 Jun 25.....	CASLEO 2.15 m	$\lambda\lambda 4700\text{--}7200$	3600	PA 90° : southern nucleus
		$\lambda\lambda 4700\text{--}7200$	3600	PA 90° : northern nucleus

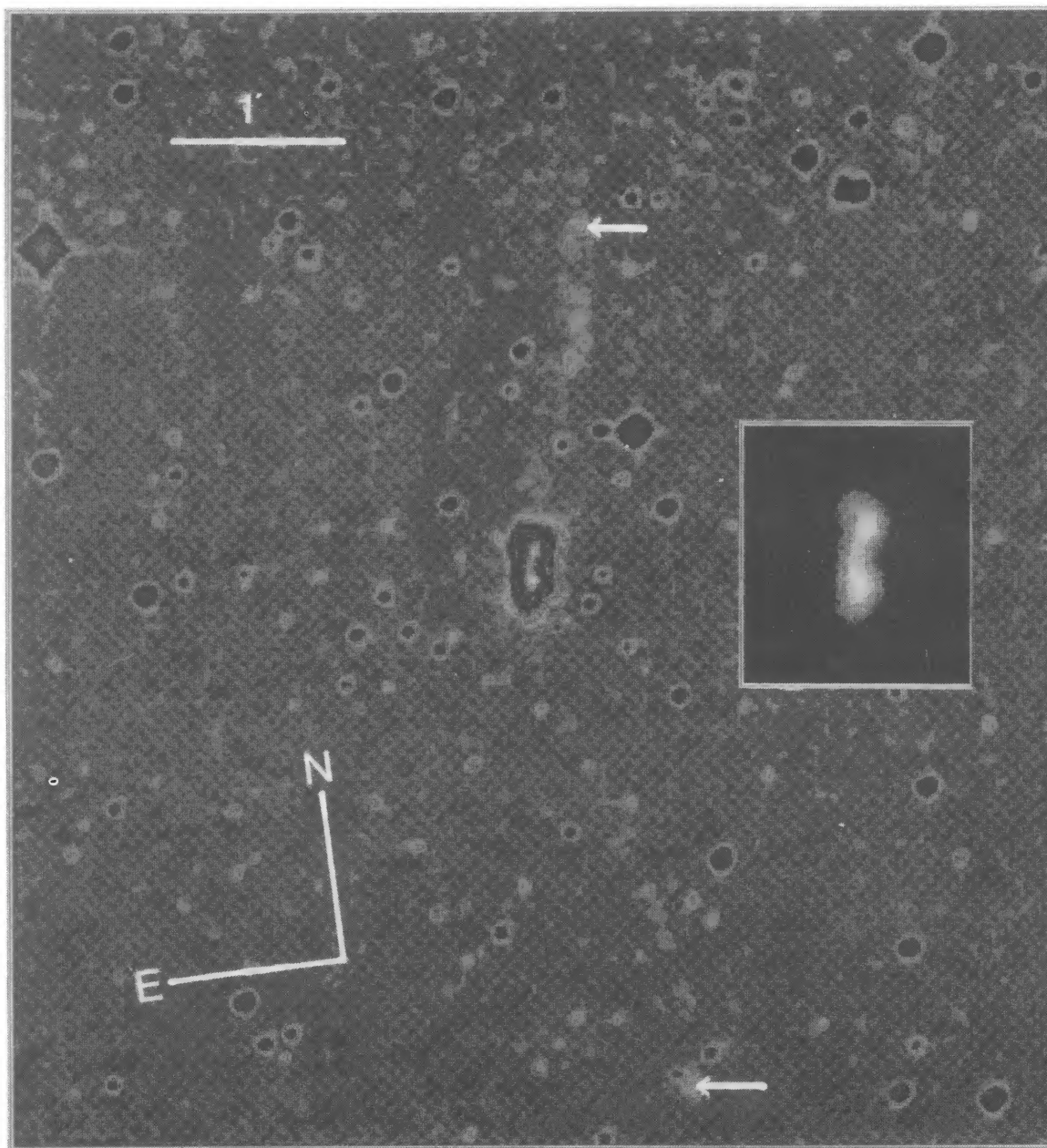


FIG. 1.—Digitized image of the optical counterpart of IRAS 19254–7245 and its environment. The image has been obtained using the Guide Star Astrometric Package (GASP) of the STScI. It is clear the presence of the two elongated tails with a total projected size of around 305 kpc if $H_0 = 75 \text{ km s}^{-1} \text{ Mpc}^{-1}$ is assumed. COLINA, LÍPARI, & MACCHETTO (see 379, 114)

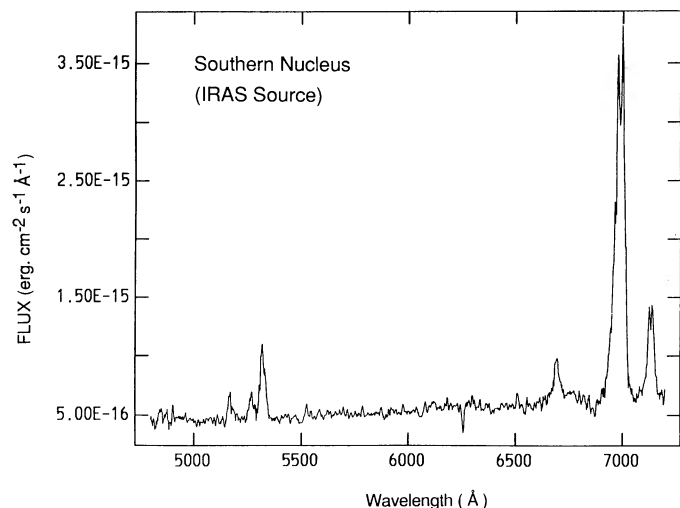


FIG. 2a

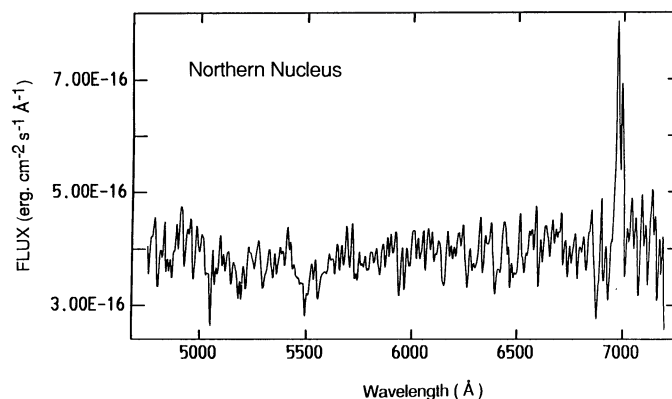


FIG. 2b

FIG. 2.—(a) Calibrated optical spectrum through a $3'' \times 6''$ aperture of the southern nucleus of the galaxy IRAS 19254–7245. This nucleus corresponds in position with the *IRAS* emission peak and shows a characteristic Seyfert 2-type spectrum. (b) Calibrated optical spectrum of the northern nucleus of IRAS 19254–7245 using the same aperture. Only $H\alpha$ and $[N\ II]$ are detected in emission.

However, in our particular case, there are some uncertainties in the extinction determination using the Balmer lines that one must bear in mind. The first relates to the strong blending of the $H\alpha$ and $[N\ II]$ emission lines; different combinations on the number of individual components gave similar total intensities within a 10%–15% uncertainty. Given a similar uncertainty in the $H\beta$ flux due to its poorer S/N, this measured extinction could be in error by $\sigma E(B-V) = \pm 0.20$. The second effect affects the absolute value of the extinction. If collisional excitation effects are important (as could well be the case if shocks are a main excitation mechanism or if IRAS 19254–7245 is a strong soft X-ray source; see § 3.3.4), the expected theoretical $H\alpha/H\beta$ ratio would increase to around 3.0 and therefore the extinction $E(B-V)$ would decrease to a value $E(B-V) = 1.34$.

To be consistent with previous extinction estimates by other authors and since the absolute change in the $E(B-V)$ value due to collisional effects is smaller than the uncertainty due to our spectral resolution, we will consider throughout the paper an internal extinction characterized by $E(B-V) = 1.40 \pm 0.20$.

Although we cannot trace the dust distribution using our single-aperture spectroscopy, we could have an upper limit to the total amount of dust M_d present in this galaxy if we assume that the total far-infrared luminosity comes from reprocessed radiation by dust in thermal equilibrium with its surrounding radiation field. Therefore:

$$M_d = \frac{d\rho_d L_{\text{FIR}}}{3Q_{\text{abs}}(T_d)\sigma T_d^4} \quad (1)$$

if spherical optically thin grain particles are considered. In this formula, d represents the typical grain radius ($= 0.1\ \mu\text{m}$; Hildebrand 1983), ρ_d represents the grain density ($= 3\ \text{g cm}^{-3}$; Hildebrand 1983), Q_{abs} is the grain emissivity (Draine & Lee 1984), σ is the Stefan-Boltzmann constant, and T_d is the grain temperature ($= 35\ \text{K}$; obtained using the *IRAS* $100\ \mu\text{m}$ over $60\ \mu\text{m}$ flux ratio and assuming a dust emissivity proportional to λ^{-2}). $L_{\text{FIR}} = 1.66 \times 10^{45}\ \text{ergs s}^{-1}$ is the far-infrared luminosity using the *IRAS* prescription (Catalogued Galaxies in the *IRAS* Survey, Version 2 1989).

The total amount of dust measured in this way is $M_d = 1.5 \times 10^7 M_\odot$. If a gas–dust ratio of 200 is assumed (typical of $H\ II$ regions; Spitzer 1968), the total amount of cool gas in this galaxy will be of the order of $M_{\text{cg}} = 3.0 \times 10^9 M_\odot$, while the total amount of molecular gas detected in the whole system corresponds to $M_{\text{H}_2} = 3.0 \times 10^{10} M_\odot$ (Mirabel et al. 1990).

3.3. Physical Properties of the Ionized Gas

3.3.1. Electron Density and Temperature

The electron density of the ionized gas was calculated using the standard $[S\ II]\ \lambda 6717$ versus $[S\ II]\ \lambda 6731$ emission-line ratio (see Aller 1984). The measured density of $N_e = 670\ \text{cm}^{-3}$ corresponds to typical values of densities in emission-line regions close to the nuclei of active galaxies. Therefore, since we are using an aperture of $3'' \times 6''$ (i.e., $3.5 \times 7\ \text{kpc}$ at the IRAS 19254–7245 redshift) and the emissivity of collisional lines depends on N_e^2 , this value has a strong bias toward the more central regions assuming there is a radial electron density gradient (as observed in some other galaxies like IC 5063: Colina, Sparks, & Macchetto 1991; M82 and NGC 3256; Heckman et al. 1990).

On the other hand, we were not able to measure the electron temperature using the standard $[O\ III]\ \lambda 4959 + \lambda 5007$ versus $[O\ III]\ \lambda 4363$ line ratio (Aller 1984) since our spectrum did not cover the spectral region below $4500\ \text{\AA}$ (rest frame). However, the electron temperature measured in several emission-line regions around different radio galaxies and active galaxies ranges from $T_e = 10^4$ to $2 \times 10^4\ \text{K}$ (Robinson et al. 1987). Also, different excitation mechanisms, like nonthermal power-law and radiative shocks, give an equilibrium electron temperature ranging from 10^4 to $2.5 \times 10^4\ \text{K}$ when a good match with the observed emission-line spectrum is obtained. Therefore, we will consider throughout the paper a mean electron temperature of $T_e = 1.5 \times 10^4\ \text{K}$.

3.3.2. Kinematical Components

Our spectrum of the southern optical nucleus (see Fig. 2a) shows that all emission lines are formed by several different

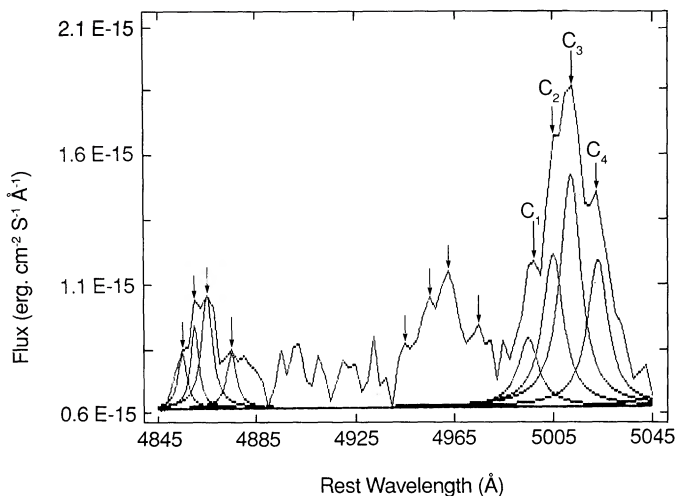


FIG. 3.— $H\beta$ and $[O\text{ III}]$ 4959, 5007 Å emission-line profiles showing the four independent kinematical components. These have a maximum velocity separation of 1491 km s^{-1} and are explained in terms of a biconical outflow model (see text for details).

components. This is particularly clear in the strong and isolated $[O\text{ III}]$ 5007 Å emission line (Fig. 3), although the same components can also be found in the $H\beta$ and $[O\text{ I}]$ 6300 Å emission lines. The characteristics of each component in terms of its absolute velocity and the amount of relative flux carried are shown in Table 2. Also indicated is the velocity difference relative to the galaxy itself, where the last has been measured using the NaD absorption line and has a value of $V_{\text{sys}} = 17,900\text{ km s}^{-1}$. The contribution of each of the four kinematical components to the different emission lines is shown in Table 3. In this table, footnotes a–d indicate the total flux corresponding to the sum of the components where our resolution was not good enough to distinguish the individual components.

The observed velocity difference of the four detected components of the $[O\text{ III}]$ λ 5007 emission line amounts to $+1491\text{ km s}^{-1}$. Velocity differences like these are also found in the double peak profile of the emission lines in high and ultra-luminous *IRAS* galaxies where typical velocity differences are in the range of 300 to 600 km s^{-1} (Heckman et al. 1990). These authors only found a case, NGC 3079, where a velocity range of over 2000 km s^{-1} was detected. These well-separated kinematical components are also similar to those observed in the

TABLE 2
VELOCITY OF THE EMISSION-LINE COMPONENTS^a

Component	I/I^b	$V_{H\beta}$	$V_{[O\text{ III}]}$	$V_{[O\text{ I}]}$	$V_{[O\text{ III}]} - V_{\text{sys}}^c$
C_1	11.2	17308	17223	17280	-677
C_2	26.0	17731	17730	17674	-170
C_3	38.5	18124	18096	18012	+196
C_4	24.3	18694	18714	(18505)	+814

^a Velocities are in units of km s^{-1} and have been obtained using the expression $1+z = [(c+V)/(c-V)]^{0.5}$.

^b This column represents the fraction of emission-line flux that goes into each independent component as measured using the $[O\text{ III}]$ 5007 Å line.

^c The system velocity has been obtained using the Na D absorption line.

TABLE 3
MEASURED EMISSION-LINE FLUX^a

Line	C_1	C_2	C_3	C_4	Total
$H\beta$	1.2	2.0	2.2	1.7	7.1
$[O\text{ III}]$ 5007.....	3.8	8.8	13.0	8.2	33.8
$[O\text{ I}]$ 6300.....	2.6	8.3	9.8	4.7	25.4
$[N\text{ II}]$ 6548.....	6.3	^b	^b	^b	40.1
$H\alpha$	^c	^c	^c	^c	92.1
$[N\text{ II}]$ 6584.....	^d	^d	^d	19.6	122.0
$[S\text{ II}]$ 6717.....	2.4	^e	^e	^e	20.1
$[S\text{ II}]$ 6731.....	^f	^f	^f	4.9	22.3

^a Flux is given in units of $10^{-15}\text{ ergs cm}^{-2}\text{ s}^{-1}$ without internal reddening correction.

^b Sum of components C_2 , C_3 , and C_4 : 33.8.

^c Sum of all components: 92.1.

^d Sum of components C_1 , C_2 , and C_3 : 102.4.

^e Sum of components C_2 , C_3 , and C_4 : 17.7.

^f Sum of components C_1 , C_2 , and C_3 : 17.4.

nearby Seyfert 2 galaxy NGC 4388 (Colina et al. 1987) where five different components separated up to 580 km s^{-1} in velocity were detected. The interpretation of the line splitting in terms of a biconical flow generated in a large process of star formation will be discussed in §§ 4.2 and 4.3.

The observed CO emission-line profile (Mirabel et al. 1990) extends over a range of 800 km s^{-1} in velocity and shows a blue asymmetry. The profile of this shows also two peaks at around $cz \approx 18,300\text{ km s}^{-1}$ and $cz \approx 18,550\text{ km s}^{-1}$, respectively. Since the CO observations have a FWHM resolution of $44''$, it is not clear if these velocity peaks correspond to our component C_2 , $cz = 18,314\text{ km s}^{-1}$, and to our system velocity obtained using the Na D absorption line, $cz = 18,470\text{ km s}^{-1}$.

3.3.3. Amount and Distribution of Ionized Gas

The mass and filling factor of the ionized gas in these emission line regions can be obtained as a function of the $H\beta$ and $[O\text{ III}]$ luminosities using the following expressions:

$$M_g = \begin{cases} 1.24 \times 10^{-32} L(H\beta) N_e^{-1} M_\odot \\ 3.28 \times 10^{-33} L([O\text{ III}]) N_e^{-1} M_\odot \end{cases} \quad (2)$$

$$f = \begin{cases} 3.55 \times 10^{-40} L(H\beta) N_e^{-2} l^{-1.5} a^{-1.5} \\ 9.78 \times 10^{-41} L([O\text{ III}]) N_e^{-2} l^{-1.5} a^{-1.5} \end{cases}, \quad (3)$$

where an O^{++} abundance of $N(O^{++}) = 4.48 \times 10^{-5} N(H^+)$ has been considered and where l and a are the projected dimensions in kpc (3.5×3.5) and N_e is the electron density as given in § 3.2. The results are shown in Table 4. While the amount of gas and filling factor of each kinematical component is of the order of a few times $10^7 M_\odot$ and 10^{-5} respectively, the total ionized gas mass and filling factor of the emission-line regions are of the order of $10^8 M_\odot$ and 10^{-4} , respectively. These values are similar to those observed in highly luminous radio galaxies in general (Baum & Heckman 1989). This could represent the amount and distribution of dense interstellar gas/dust clouds within the first 3–6 kpc around the nucleus of gas-rich galaxies which are in the advanced stages of the merging process.

3.3.4. Excitation Conditions

Excitation conditions in the emission-line regions can be compared and parameterized (through the usual ionization parameter $U = N_{\text{ph}}^{\text{ion}} [4\pi R^2 N_e c]^{-1}$) using the various line

TABLE 4
PHYSICAL PROPERTIES OF THE EMISSION-LINE REGIONS

Component	$V - V_{\text{sys}}$ (km s ⁻¹)	$L_{\text{H}\beta}$ ^a (10 ⁴² ergs s ⁻¹)	$L_{[\text{O III}]}$ ^a (10 ⁴² ergs s ⁻¹)	Mass (10 ⁷ M _⊙)	Filling Factor (10 ⁻⁵)
C ₁	-677	0.94	2.54	1.5	1.54
C ₂	-170	1.57	5.90	3.0	3.02
C ₃	+196	1.73	8.74	3.9	3.95
C ₄	+814	1.33	5.52	2.6	2.70
Total	5.57	22.7	11.0	11.21

^a Values corrected by internal extinction with $E(B-V) = 1.40$.

ratios as tabulated in Table 5. This table shows the logarithm of the ratios of the strongest emission lines (He II 4686, H β , [O III] 5007, [O I] 6300, H α , [N II] 6584, and [S II] 6717, 6731) for the emission-line regions around the southern nucleus (nucleus A in Table 5) as observed and with an internal reddening correction of $E(B-V) = 1.40$ as well as the observed [N II]/H α ratio for the northern nucleus (labeled as B in Table 5). Also shown for comparison are the ratios obtained from shock-heating models (Binette, Dopita, & Tuohy 1985), and photoionization models with a nonthermal source (Stasinska 1984) or hot main-sequence stars (Evans & Dopita 1985). It is clear that none of the different ionization mechanisms alone can reproduce the observed emission-line ratios. Both the power-law nonthermal central source (Photon-3 in Table 5) or the low-velocity radiative shocks (Shock+2 in Table 5) could account for the high luminosity of the [O III] line relative to H β and [O I] but fail for the low ionization emission lines. On the other hand, typical H II simulations (H II in Table 4) fail completely in giving any good account of the observed line ratios.

The different line ratios using Veilleux & Osterbrock (1987) diagnostic diagrams are shown in Figure 4 which also includes the line ratios from Sanders's sample of ultraluminous infrared galaxies (values from Table 5 of Sanders et al. 1988 with reddening correction). It is clear from these plots that IRAS 19254-7245 has the same typical spectrum of ultraluminous infrared galaxies and that occupies a place within the low-excitation end of Seyfert 2-type nucleus.

Altogether, this suggests that the ionization source in IRAS 19254-7245, and in ultraluminous galaxies in general, could

be a complex function of different excitation mechanisms, i.e., obscured central power-law source, extended hot star radiation field, and perhaps less important radiative shocks generated in superwinds (see § 3.4 and discussion § 4.4).

3.4. Ionizing Source

Finally, we can characterize the intrinsic power of the ionizing source using the measured H α luminosity corrected by internal reddening. Therefore, the total number of ionizing photons measured in the emission-line regions would be given by the expression (Osterbrock 1989)

$$N_{\text{ph}} = \frac{\alpha_{\text{B}}(\text{H}^0, T)}{\alpha_{\text{eff}}^{\text{H}\alpha}(T)} \frac{L(\text{H}\alpha)}{h\nu_{\text{H}\alpha}} \Omega^{-1} \\ = 7.52 \times 10^{11} L(\text{H}\alpha) \Omega^{-1} \text{ photons s}^{-1} \quad (4)$$

if an electron temperature of 15,000 K and no collisional effects are assumed. In this expression Ω represents the covering factor of the gas clouds over the ionizing source. Considering the total H α luminosity measured in these regions $L(\text{H}\alpha) = 1.6 \times 10^{43}$ ergs s⁻¹, we get a lower limit to the total number of ionizing photons of $N_{\text{ion}} = 1.2 \times 10^{55}$ photons s⁻¹ if the covering factor equals unity. Therefore, the type of ionizing source needed to explain both the emission-line luminosities and the observed excitation conditions must produce a large amount of ionizing photons in absolute terms and must have a large fraction of these ionizing photons with energies greater than the O⁺⁺ ionization level, i.e., 35.1 eV. As discussed in § 4.4, these conditions can be obtained by a combination of a large

TABLE 5
MEASURED AND DEREDDENED EMISSION-LINE RATIOS

Nucleus	log ([O III]/H β)	log ([O I]/[O III])	log ([O I]/H α)	log ([N II]/H α)	log ([S II]/H α)
A	0.68	-0.12	-0.56	0.12	-0.34
A ^a	0.61	-1.03	-0.36	0.11	-0.38
B	-0.18	...
H II ^b	0.12	-1.94	-2.28	-0.65	-1.22
Photon-3 ^c	0.93	-1.31	-0.85	-0.13	-0.21
Photon-4 ^c	-0.40	0.48	-0.39	0.10	0.32
Shock+2 ^d	0.73	-0.88	-0.64	-0.08	0.10
Shock+3 ^d	-0.32	1.29	0.50	0.24	0.57

^a Corrected for internal reddening with $E(B-V) = 1.40$.

^b H II region photoionization model from Evans & Dopita 1985 characterized by an ionization parameter of $U = 3 \times 10^{-3}$, an ionizing temperature $T_{\text{ion}} = 4 \times 10^4$ K and solar abundances.

^c Nonthermal photoionization models from Stasinska 1984 characterized by a spectral index of $\alpha = 1.5$, an electron density of $N_e = 10^3$ cm⁻³, solar abundances, and ionization parameter of $U = 10^{-3}$ and 10^{-4} , respectively.

^d Radiative shock models B53 and B72 of Binette, Dopita, & Tuohy 1985. Model B53 is characterized by $V_{\text{shock}} = 116$ km s⁻¹, $N_e([\text{S II}]) = 270$ cm⁻³, $T_e([\text{O III}]) = 26,900$ K, and solar abundances. Model B72 is characterized by $V_{\text{shock}} = 1080$ km s⁻¹, $N_e([\text{S II}]) = 70$ cm⁻³, $T_e([\text{O III}]) = 10,800$ K, and solar abundances.

number of hot stars and a powerful obscured nonthermal source.

4. DISCUSSION

4.1. *IRAS 19254–7245 as a Merger of Two Gas-rich Galaxies*

The optical image of IRAS 19254–7245 (Fig. 1) gives us some clues about the kind of galaxies involved in the collision and the time since this interaction started. The fact that the two tails are almost equal in size is evidence that the mass ratio of the two galaxies involved in the collision must be equal or very close to one (Toomre & Toomre 1972). Since CO measurements together with our estimates of the cold gas present in the system (see § 3.2) give values of the order of $10^{10} M_{\odot}$, this indicates that the two original galaxies involved in the collision were two equally massive gas-rich spiral galaxies.

Since the extraordinary large tails show almost no curvature, this suggests that we are viewing the system almost edge-on (the plane of the orbit has an inclination with respect to our line of sight of around 20° – 30°). This estimate agrees with an independent value obtained from the biconical outflow geometry where we found the symmetry axis of the outflow to be almost perpendicular to our line of sight (see § 4.2).

Finally, the size of the tails can give us an idea of when the interaction did start. If an escape velocity of around 100 km s^{-1} is assumed for the material in the tails (Borne & Richstone 1991), considering a mean projected size of around 150 kpc, we obtain a value of $1.2 \times 10^9 \text{ yr}$ since the interaction began.

It is important to remark that if the interaction has generated the starburst/AGN activity we are observing in this galaxy, this must have occurred very late in the history of the interaction. If this was not the case, first we would expect to see an absorption spectrum characteristic of an underlying old stellar population, and second, we would need to have an impressively large initial amount of gas of $2 \times 10^{11} M_{\odot}$ to produce the derived steady star formation rate (see § 4.3).

It is interesting to note the overall morphological similarities between the “Superantennae” and Arp 226 (Schwiezer 1982; also recently modeled in detail by Borne & Richstone 1991), even at the level of the presence of condensations along the tails. Therefore, it would be important to investigate if these condensations are starburst regions, and, if so, if their existence is a general characteristic of strong interacting systems formed by gas-rich galaxies.

4.2. *IRAS 19254–7245 as a Superbubble/Superwind Generator*

The four independent kinematical components clearly detected in the $[\text{O III}] 5007 \text{ \AA}$ emission line (see Fig. 3 and § 3.3.2) can be modeled as a biconical outflow expanding into the halo of a spiral galaxy and with an opening angle θ and symmetry axis inclined an angle i with respect to our line of sight (for a detailed theoretical and observational account of the presence of such winds in highly luminous *IRAS* galaxies, we refer the reader to Heckman et al. 1990 and references therein).

Assuming this geometry and considering that the residual velocities ($V_{[\text{O III}]} - V_{\text{sys}}$ in Table 2) are the projected line-of-sight velocities, we obtain an inclination angle of $i = 77^{\circ}$ and a flow velocity of $V_{\text{flow}} = 880 \text{ km s}^{-1}$ if an opening angle of $\theta = 70^{\circ}$ is considered; or $i = 69^{\circ}$ and $V_{\text{flow}} = 765 \text{ km s}^{-1}$ if $\theta = 90^{\circ}$. Therefore, in the following sections we will assume

an intermediate value of $V_{\text{flow}} \approx 800 \text{ km s}^{-1}$, $i \approx 73^{\circ}$ and $\theta \approx 80^{\circ}$.

The amount of detected ionized gas (see § 3.3 and Table 4) combined with the flow velocity derived above indicates the presence of a powerful energy source capable of moving interstellar gas clouds with a total mass of $10^8 M_{\odot}$ at velocities of 800 km s^{-1} using a fraction of its total energy. We will propose in the following section that the most likely physical mechanism capable of generating such an enormous amount of kinetic energy is a huge starburst via supernova explosions and stellar winds.

Another alternative to explain the existence of the four kinematical components detected in the emission-line profiles could be that these are associated with four independent remnants of the original merging galaxies, i.e., large sections of disks. We do not believe this is a valid hypothesis. First, our aperture is centered in the nucleus of IRAS 19254–7245 and has a size (see § 2) that covers only short distances, up to 3 kpc, around the nucleus. Second, detailed observational (Schwiezer 1982) and theoretical work (Borne & Richstone 1991) on Arp 226 reveals a system similar to the “Superantennae”: a merger of two gas disk galaxies viewed almost edge-on and with a messy central part and long tails. For Arp 226, velocity measurements along the major and minor axes show velocity differences of only 100 km s^{-1} with respect to the system (Schwiezer 1982).

4.3. *IRAS 19254–7245 as a Starburst Galaxy*

Current estimates of the star formation rates in highly luminous infrared galaxies make use of the observed infrared and/or $\text{H}\alpha$ luminosities (Heckman et al. 1990). Assuming a Salpeter IMF and a constant SFR over time scales of $2 \times 10^7 \text{ yr}$ (main-sequence lifetime of stars more massive than $10 M_{\odot}$), Hunter (1986) obtains the following expressions:

$$\text{SFR}(L_{\text{IR}}) = 6.7 \times 10^{-44} \beta^{-1} L(\text{IR}) M_{\odot} \text{ yr}^{-1} \quad (5)$$

$$\text{SFR}(L_{\text{H}\alpha}) = 7.1 \times 10^{-42} \eta^{-1} L(\text{H}\alpha) M_{\odot} \text{ yr}^{-1}, \quad (6)$$

where β and η are the fraction of ionizing photons converted into infrared and $\text{H}\alpha$ photons respectively. Therefore, considering $\beta = \eta = 0.5$, the far-infrared luminosity in the range 8–1000 μm equal to $\log L(\text{IR}) = 45.57 \text{ ergs s}^{-1}$ (obtained using the four *IRAS* band fluxes and Perault prescription kindly made available to us by D. Sanders) and $\log L(\text{H}\alpha) = 43.19 \text{ ergs s}^{-1}$, we obtain for IRAS 19254–7245 star formation rates of $\text{SFR}(L_{\text{IR}}) = 498 M_{\odot} \text{ yr}^{-1}$ and of $\text{SFR}(L_{\text{H}\alpha}) = 221 M_{\odot} \text{ yr}^{-1}$ respectively.

This method is based on the assumption that all the available ionizing photons come only from newly formed hot stars. This hypothesis can be reasonably good for moderately and highly luminous *IRAS* galaxies presenting an H II region-type spectrum (Leech et al. 1989). However, for the particular case of IRAS 19254–7245, as well as for most ultraluminous *IRAS* galaxies, this assumption could well not be completely true. As shown in the emission-line ratio diagrams (Fig. 4), IRAS 19254–7245 is located in the Seyfert 2 region, indicating that the ionizing source must have enough high-energy photons (energies greater than 35 eV) to produce the observed $[\text{O III}]/\text{H}\beta$ ratio. This indicates that in addition to the hot stars, there is another source that must contribute substantially to the ionization of the gas clouds. Therefore, one must consider the previous SFR estimates as an upper limit to the true star formation rate.

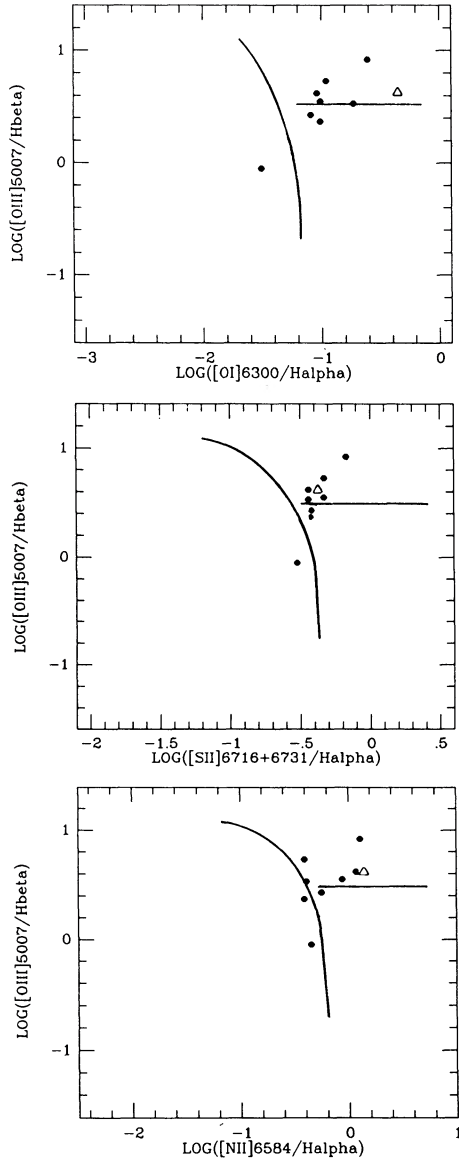


FIG. 4.—Reddening-corrected emission-line ratios for IRAS 19254–7245 (open triangle) together with those for ultraluminous IRAS galaxies (obtained from the extinction-corrected values in Table 5 of Sanders et al. 1988). The curved lines indicated the H II–AGN separation in these diagrams (Veilleux & Osterbrock 1987), while the line parallel to the horizontal axis represents the separation between LINERs and Seyfert-type spectra. It is clear from these plots that IRAS 19254–7245 has similar AGN excitation conditions to the rest of the ultraluminous IRAS galaxies.

In the following we will present an alternative way of determining the star formation rate based on our measurements of the kinetic energy generated in the bulk motion of the ionized ISM clouds.

Assuming the biconical outflow model to be correct (see § 4.2), we can measure the kinetic energy in the emission-line clouds as $E_k^{\text{flow}} = 0.5 M_g V_{\text{flow}}^2$ and compare this value with what would be expected from the wind mass-loss and supernova explosions of massive stars in a starburst scenario. The obtained kinetic energy of the flow is $E_k^{\text{flow}} = 1.4 \times 10^{57}$ ergs, where $M_g = 1.1 \times 10^8 M_\odot$ (see § 3.3.2) and $V_{\text{flow}} = 800 \text{ km s}^{-1}$ (see § 4.2).

Now, we calculate the total amount of kinetic energy liberated by massive stars. We will assume a Salpeter IMF ($\alpha = 2.35$) with stars in the range $0.1 \leq M_* \leq 100 M_\odot$ and a steady SFR over $t_{\text{SFR}} = 2 \times 10^7$ yr (time scale needed for a $10 M_\odot$ star to leave the main sequence and evolve to the final stages of supernova explosion). Therefore:

$$M_T(t=0) = \text{SFR } t_{\text{SFR}} = A \int_{0.1 M_\odot}^{100 M_\odot} m \cdot m^{-\alpha} dm \quad (7)$$

Under our simplified model, we consider that three independent components, namely the supernova explosions, Wolf-Rayet winds, and hot main-sequence stars, contribute to the total kinetic energy liberated in the star formation process. We should include as a fourth component, the winds generated by the post-main-sequence stars, but so far there is no analytical expression for the velocity of these flows. However, although the mass loss during this phase is larger than during the main-sequence phase, since the time scale is shorter and the flow velocity smaller than during the main-sequence phase, we do not believe this contribution would change our conclusions about the SFR by factors larger than 2. Therefore, the general expression will be

$$E_k^{\text{starburst}} = E_k^{\text{SN}} + E_k^{\text{WR}} + E_k^{\text{MS}}. \quad (8)$$

The first contributor is associated with the supernova explosions. We consider that all stars more massive than $10 M_\odot$ have had enough time to evolve up to the supernova phase. Therefore, assuming a mean energy of $\langle E^{\text{SN}} \rangle = 7.5 \times 10^{50}$ ergs liberated in both Type I and Type II supernovae (Chevalier 1977), we obtain:

$$\begin{aligned} E_k^{\text{SN}} &= \langle E^{\text{SN}} \rangle \int_{10 M_\odot}^{100 M_\odot} A m^{-\alpha} dm \\ &= 8.14 \times 10^{55} \cdot \text{SFR ergs} \end{aligned} \quad (9)$$

where A is obtained as a function of SFR from equation (7). The second and third contributors correspond to mass loss of massive stars in their main-sequence and W-R phases. According to Abbott (1982) for stars more massive than $60 M_\odot$ the O star phase dominates the total wind energy, while for stars less massive, the W-R phase dominates. Assuming a mean kinetic energy for the W-R phase $\langle E^{\text{WR}} \rangle = 5 \times 10^{50}$ ergs (Abbott 1982), we obtain

$$\begin{aligned} E_k^{\text{WR}} &= \langle E^{\text{WR}} \rangle \int_{25 M_\odot}^{100 M_\odot} A m^{-\alpha} dm \\ &= 1.39 \times 10^{55} \cdot \text{SFR ergs} \end{aligned} \quad (10)$$

and

$$\begin{aligned} E_k^{\text{MS}} &= 0.5 \int_{10 M_\odot}^{100 M_\odot} A m^{-\alpha} \dot{m}_w t_{\text{MS}} v_w^2 dm \\ &= 3.11 \times 10^{55} \cdot \text{SFR ergs}, \end{aligned} \quad (11)$$

where \dot{m}_w , t_{MS} , and v_w are the analytical expressions of mass-loss rates, main-sequence lifetime, and wind velocities obtained by Elson, Fall, & Freeman (1989) for stars in the mass range 10 – $100 M_\odot$ from the empirical results of Abbott (1982):

$$\dot{m}_w = 5.76 \times 10^{-15} m^5 M_\odot \text{ yr}^{-1} \quad (12)$$

$$t_{\text{MS}} = 1.20 \times 10^8 m^{-0.9} \text{ yr} \quad (13)$$

$$v_w = 1.86 \times 10^3 m^{0.14} \text{ km s}^{-1}. \quad (14)$$

Finally, to obtain the SFR we need to consider an efficiency factor which equals the fraction of the total available kinetic energy which goes into bulk motion. According to Abbott (1982) these efficiency factors are $\epsilon^{\text{SN}} \approx 0.06$ for supernovae and $\epsilon^{\text{WR}} = \epsilon^{\text{MS}} \approx 0.10$ for mass-loss winds. Therefore:

$$E_k^{\text{flow}} = \epsilon E_k^{\text{starburst}} = \epsilon^{\text{SN}} E_k^{\text{SN}} + \epsilon^{\text{WR}} E_k^{\text{WR}} + \epsilon^{\text{MS}} E_k^{\text{MS}} \quad (15)$$

substituting the values of previous expressions we obtain a star formation rate $\text{SFR} = 150 M_{\odot} \text{ yr}^{-1}$. This value is a factor about 2 smaller than the previous SFR estimates using the H α and far-infrared luminosities. However, within the implicit uncertainties in all these different SFR determinations (time scale over which SFR has taken place, energy conversion factors, lower limit of the massive stars, IMF, ...), we consider that our method agrees with those based on luminosity measurements.

The basic conclusion is that the presence of a starburst with a large star formation rate of $\text{SFR} = 150 M_{\odot}$ and in a relatively small spatial scale (of the order of 3 kpc in radius) is sufficient to explain the kinetic energy measured assuming our biconical outflow model. However, this model has a strong prediction that could rapidly be checked: the number of supernova explosions per year will be around four. Therefore, if the starburst hypothesis is true, we should be able to detect supernova explosions in this galaxy using deep CCD images.

4.4. IRAS 19254–7245 as a Hidden Quasar

Since the ultraluminous IRAS galaxies have bolometric luminosities similar to these of the more luminous quasars but shifted to infrared wavelengths, we will discuss in the following the need for a centrally obscured nonthermal source to explain the high excitation together with the extraordinarily large luminosities detected in IRAS 19254–7245.

To do that, we will check first if the amount and energy distribution of the ionizing photons (N_{ion}^*) liberated by the massive ($M^* \geq 20 M_{\odot}$) main-sequence stars under the previous star formation scenario (see § 4.3) are sufficient to explain the total number of ionizing photons (N_{ph}) needed to generate the H α luminosity (see § 3.4). Also, assuming a mean photon energy and a one-to-one conversion rate of UV photons into infrared photons due to reradiation by dust, a comparison with the far-infrared luminosity (L_{FIR} in § 3.2) will be made.

Considering a mean photon energy of $\langle h\nu \rangle = 20$ eV and a mean number of ionizing photons per O star $N_{\text{ion}}^{\text{mean}} = N_{\text{ion}}(\text{O6}) = 1.69 \times 10^{49}$ photons s^{-1} (Osterbrock 1989), the total number of ionizing photons will be given by

$$N_{\text{ion}}^* = N^*(20-100 M_{\odot}) N_{\text{ion}}^{\text{mean}} \text{ photons } \text{s}^{-1} \quad (16)$$

$$N_{\text{ion}}^* = \frac{\text{SFR} \cdot t_{\text{SFR}}}{\int_{0.1 M_{\odot}}^{100 M_{\odot}} m^{-\alpha} dm} \int_{20 M_{\odot}}^{100 M_{\odot}} m^{-\alpha} dm N_{\text{ion}}^{\text{mean}} \text{ photons } \text{s}^{-1} \quad (17)$$

Consequently using the star formation parameters of § 4.3, we obtain $N_{\text{ion}}^* = 1.0 \times 10^{56}$ photons s^{-1} and $L_{\text{ion}}^* = N_{\text{ion}}^* \langle h\nu \rangle = 3.22 \times 10^{45}$ ergs s^{-1} . These values agree within 15% with those obtained by detailed models of massive H II regions with total masses of $3 \times 10^9 M_{\odot}$ (M. Vargas & A. Díaz, private communication) while being a factor of 10 above the results obtained using analytical expressions for the amount of ionizing photons as a function of stellar masses (Gallagher, Hunter, & Tutukov 1984). Also, our results are a factor 2–3 smaller than those obtained by detailed steady state star for-

mation models using evolutionary tracks and models of stellar atmospheres (C. Leitherer, private communication).

The number of photons N_{ion}^* is consistent with the value obtained from the H α measurements if the covering factor equals 1 (see § 3.3.3) while the corresponding ionizing luminosity L_{ion}^* agrees with the measured infrared luminosity (L_{FIR} in § 3.2). Therefore, based on emission line and infrared luminosities, there would be no need to invoke an additional ionization source.

However, the fraction of ionizing photons with energies above the O^{++} ionization level (35.1 eV) corresponds to 3% or 9% of the total number of photons above the Lyman limit using H II region evolutionary models (M. Vargas & A. I. Díaz, private communication) or starburst evolutionary models (C. Leitherer; private communication), respectively. None of these fractions of hard photons are enough to explain the observed Seyfert 2-type emission-line spectrum, in particular the [O III]/H β ratio. However, one could generate hard photons if the existence of very hot and massive post-main-sequence stars (Warmers hypothesized by Terlevich & Melnick 1985) is considered. According to new models (M. Vargas & A. Díaz, private communication), a starburst of $1-5 \times 10^9 M_{\odot}$ would generate Warmers after 3.5×10^6 yr, and these will last for about 2×10^6 yr. During this phase, the starburst will generate an ionizing luminosity of $L_{\text{ion}}^* \approx 1.3-6.6 \times 10^{45}$ ergs s^{-1} , but now 21% of the corresponding ionizing photons will have energies above 35.1 eV, and it will be able to create a Seyfert 2-type spectrum. However, the main problem with this idea is the lifetime scale of the Warmers. This is very short (of the order of a million years) and therefore the possibility to observe this phenomenon would be rather small (1% of all strongly interacting pairs of gas-rich spirals). Anyway, we believe that it is a promising hypothesis that needs to be worked out in more detail.

In conclusion, under the starburst scenario and leaving aside the Warmer hypothesis, there is a lack of energetic photons that could generate high excitation conditions.

The only alternative to solve these problems is to consider, as already suggested by Sanders et al. (1988), the presence of an obscured highly luminous quasar nucleus at the center of IRAS 19254–7245 with an ionizing luminosity of the order of 10^{45} ergs s^{-1} , i.e., $N_{\text{ion}}^{\text{QSO}} = 2 \times 10^{55}$ photons s^{-1} and mean energy of 35 eV. This idea would agree with the location of IRAS 19254–7245 in the IRAS color-color diagram. With $\alpha(100, 60) = -0.35$ and $\alpha(60, 25) = -1.49$, it is located near the blackbody region with a temperature higher than the temperatures of the starburst galaxies (Sekiguchi 1987).

In conclusion, the observed luminosities and excitation conditions are consistent with a scenario where the central luminous nonthermal continuum source (quasar-type nucleus) is obscured by a large amount of gas dust clouds where the massive star formation is taking place. These clouds would transform the nonthermal continuum into a blackbody infrared spectrum with a temperature higher than that of the starburst galaxies.

To be able to quantify the relative importance of the nonthermal source and starburst in the heating and ionization of the surrounding interstellar medium, we need first to constrain the starburst scenario more precisely. This can be done through a careful search for supernova explosions in this galaxy since we expect to have four supernovae a year according to our model. If none is detected, the whole idea of the starburst scenario should be reconsidered.

5. CONCLUSIONS

We have presented in this paper for the first time aperture spectroscopy of the ultraluminous infrared galaxy IRAS 19254–7245 together with an image of the galaxy and its surroundings. From these data the following conclusions can be reached:

1. IRAS 19254–7245 morphology clearly indicates that it is the product of the interaction of two galaxies. The almost equally long tails with a total size of 305 kpc, the distorted main body showing the presence of two well-defined independent nuclei, and the large amount of gas indicate that the interaction started 10^9 yr ago and that the galaxies involved in the interaction are two similar massive gas-rich spirals.

2. The mass of the ionized gas in the emission-line regions amounts to $M_g = 1.1 \times 10^8 M_\odot$ while the upper limit to the total amount of cold gas associated to dust heated by the ionization source is $M_{cg} = 3 \times 10^9 M_\odot$. This is a factor of 10 less than the total amount of molecular gas detected by Mirabel and collaborators.

3. IRAS 19254–7245 has emission lines formed by four different and kinematically independent components separated by a maximum velocity of 1491 km s^{-1} . This behavior has been interpreted as a biconical outflow model characterized by an opening angle of 80° , and inclination of the symmetry axis of 73° with respect to our line of sight, and a flow velocity of 800 km s^{-1} . Under this model, the total amount of kinetic energy in the form of bulk motion of the emission-line regions is $E_k^{\text{flow}} = 1.4 \times 10^{57}$ ergs.

4. This kinetic energy is interpreted as produced by supernova explosions and stellar winds in a massive star formation process lasting $t_{\text{SFR}} = 2 \times 10^7$ yr and having a steady star formation rate of $\text{SFR} = 150 M_\odot \text{ yr}^{-1}$. The amount and energy distribution of the ionizing photons generated by the massive stars in this starburst scenario are sufficient to explain the H α and infrared luminosities but not sufficient to explain the excitation conditions IRAS 19254–7245.

5. The starburst scenario makes a strong prediction: the expected supernova explosion rate in this galaxy is four supernovae per year. Deep broad-band CCD images could be used for a careful search of supernovae in this galaxy as well as in other ultraluminous IRAS galaxies.

6. These observations are consistent with the hypothesis of a luminous quasar nucleus obscured and surrounded by large amounts of gas and dust in the form of clouds where the extraordinarily large star formation is taking place.

S. L. would like to express his gratitude to the staff members and observing assistants of CASLEO Observatory and also acknowledges partial support from CONICET during this study. L. C. wishes to acknowledge STScI hospitality during the course of this work. We are particularly grateful to N. da Costa, D. Latham, P. Pellegrini, and C. Willmer, who provided access and supplied useful information on the "Z-machine." The authors wish to thank K. Borne, A. Diaz, C. Leitherer, W. Sparks, and M. Vargas for many helpful and enlightening discussions.

REFERENCES

- Abbott, D. C. 1982, *ApJ*, 263, 723
 Aller, L. H. 1984, *Physics of Thermal Gaseous Nebulae* (Dordrecht: Reidel)
 Armus, L., Heckman, T. M., & Miley, G. 1989, *ApJ*, 347, 727
 Baum, S. A., & Heckman, T. M. 1989, *ApJ*, 336, 681
 Bevington, P. R. 1969, *Data Reduction and Error Analysis for The Physical Sciences* (New York: McGraw-Hill)
 Binette, L., Dopita, M. A., & Tuohy, I. R. 1985, *ApJ*, 297, 476
 Borne, K. D., & Richstone, D. O. 1991, *ApJ*, 369, 111
 Cataloged Galaxies and QSO Observed in the IRAS Survey, Version 2. 1989, prepared by L. Fullner & C. Lonsdale (Pasadena: JPL)
 Chevalier, R. 1977, *ARA&A*, 15, 175
 Colina, L., Fricke, K. J., Kollatschny, W., & Perryman, M. A. C. 1987, *A&A*, 186, 39
 Colina, L., Sparks, W., & Macchetto, F. D. 1991, *ApJ*, 370, 102
 da Costa, L., Pellegrini, P., Nunes, M., Willmer, C., & Latham, D. 1984, *AJ*, 89, 1310
 Davis, M., & Latham, D. W. 1979, in *Instrumentation in Astronomy III* (Proc. SPIE, Vol. 172), 71
 de Vaucouleurs, G., de Vaucouleurs, A., & Corwin, H. G. 1976, *Second Reference Catalogue of Bright Galaxies* (Austin: Univ. of Texas)
 Draine, B., & Lee, H. 1984, *ApJ*, 285, 89
 Elson, R. A. W., Fall, S. M., & Freeman, K. C. 1989, *ApJ*, 336, 734
 Evans, I. N., & Dopita, M. A. 1985, *ApJS*, 58, 125
 Fricke, K. J., & Kollatschny, W. 1989, in *IAU Symposium 134, Active Galactic Nuclei*, ed. D. E. Osterbrock & J. S. Miller (Dordrecht: Reidel), 425
 Gallagher, J. S., III, Hunter, D. A., & Tutukov, A. V. 1984, *ApJ*, 284, 544
 Heckman, T. M. 1990, in *IAU Colloquium 124, Paired and Interacting Galaxies*, ed. J. Sulentic & W. Keel (NASA CP-3098)
 Heckman, T. M., Armus, L., & Miley, G. 1990, *ApJS*, 74, 833
 Hildebrand, R. 1983, *QJRAS*, 24, 268
 Hunter, D. A., 1986, *ApJ*, 303, 171
 Latham, D. W. 1982, in *IAU Colloquium 67, Instrumentation for Astronomy with Large Optical Telescopes*, ed. C. Humphries (Dordrecht: Reidel), 259
 Lawrence, A., Rowan-Robinson, M., Leech, K., Jones, D. H. P., & Wall, J. V. 1989, *MNRAS*, 240, 329
 Leech, K., Penston, M. V., Terlevich, R., Lawrence, A., Rowan-Robinson, M., & Crawford, J. 1989, *MNRAS*, 240, 349
 Lipari, S., Bonatto, Ch., & Pastoriza, M. 1989, in *IAU VI Regional Latin-American Meeting of Astronomy* (Contribucion de la Revista Mexicana de Astronomia), in press
 ———. 1990, *MNRAS*, in press
 Lipari, S., Macchetto, F., & Golombek, D. 1991, *ApJ*, 366, L65
 Melnick, J., & Mirabel, F. 1990, *A&A*, 231, L19
 Mirabel, I. F., Booth, R. S., Garay, G., Johansson, L. E. B., & Sanders, D. B. 1990, *A&A*, 236, 327
 Osterbrock, D. E. 1989, *Astrophysics of Gaseous Nebulae and Active Galactic Nuclei* (Mill Valley: University Science Books)
 Robinson, A., Binette, L., Fosbury, R., & Tadhunter, C. 1987, *MNRAS*, 227, 97
 Sandage, A., & Tammann, G. A. 1981, *A Revised Shapley-Ames Catalogue of Bright Galaxies* (Washington, DC: Carnegie Institution)
 Sanders, D. B., Soifer, B. T., Elias, J. H., Madore, B. F., Matthews, K., Neugebauer, G., & Scoville, N. Z. 1988, *ApJ*, 325, 74
 Sekiguchi, K. 1987, *ApJ*, 316, 145
 Schweizer, F. 1982, *ApJ*, 252, 455
 Spitzer, L., Jr. 1978, *Physical Processes in the Interstellar Medium* (New York: Wiley-Interscience)
 Stasinska, G. 1984, *A&AS*, 55, 15
 Stone, R. P., & Baldwin, J. A. 1983, *MNRAS*, 204, 357
 Terlevich, R., & Melnick, J. 1985, *MNRAS*, 213, 841
 Tonry, J., & Davis, M., 1979, *AJ*, 84, 1511
 Toomre, A., & Toomre, J. 1972, *ApJ*, 178, 623
 Veilleux, S., & Osterbrock, D. E. 1987, *ApJS*, 63, 295

Note added in proof.—While this paper was in proof, I. F. Mirabel, D. Lutz, & J. Maza (*A&A*, 243, 367 [1991]) have reported long-slit spectroscopy and broad-band CCD images of the "Superantennae."

These authors also detected the presence of high-velocity and secondary [O III] components in the range 500–800 km s^{-1} relative to the system velocity. However, they indicate that these components extend up to a distance of 7" from the southern nucleus and claim that these components may represent either infalling or outflowing gas in the southern galaxy.

Mirabel and collaborators show that more than 80% of the far-infrared energy radiated by IRAS 19254-7245 comes from the southern nucleus. The *JHKL* colors measured by these authors indicate strong emission by hot dust, heated by the deeply obscured active nucleus or by a strong starburst. Therefore, their conclusions are consistent with the model presented in this paper.